Modeling the structure of clusters of C_{60} molecules

Jonathan P. K. Doye* and David J. Wales
University Chemical Laboratory, Lensfield Road, Cambridge CB2 1EW, United Kingdom

Wolfgang Branz
Max-Planck-Institut für Festkörperforschung, Heisenbergstrasse 1, D-70569 Stuttgart, Germany

Florent Calvo
Laboratoire de Physique Quantique, IRSAMC, Université Paul Sabatier, 118 Route de Narbonne, F31062 Toulouse Cedex, France
(Received 29 June 2001; published 16 November 2001)

We locate putative global minima for $(C_{60})_N$ clusters modeled by the potential of Pacheco and Prates-Ramalho up to $N=105$. These minima are based on icosahedral packing up to $N=15$, but above this size the lowest-energy structures are decahedral or close packed. Although structures based on the 98-molecule Leary tetrahedron, which have been inferred from experiment, are not lowest in energy for this potential, an examination of the energetics of a growth sequence leading to the Leary tetrahedron lends further support to the experimental assignments. An analysis of the potential energy surface topography and the thermodynamics of two example clusters indicates that the multiple-funnel topography is likely to have a strong influence on the dynamics of structure formation and that solid-solid transitions driven by differences in vibrational entropy are likely to be common.

DOI: 10.1103/PhysRevB.64.235409 PACS number(s): 61.46.+w, 36.40.Mr, 36.40.Ei

I. INTRODUCTION

There has been much interest in the condensed-phase properties of C_{60} molecules because of their unusual intermolecular potential. At high temperature the molecules can rotate freely and so they act as large ''pseudoatoms'' with interactions that are extremely short-ranged relative to the large equilibrium pair separation. Consequently the properties of C_{60} can extend beyond the range of behavior observed for atomic materials. For example, there are theoretical predictions that the liquid phase is unstable[1,2] or marginally stable[3–6] with the precise results depending on the potential (and somewhat on the methodology[7]) used.

There has also been considerable interest in the structural properties of clusters of C_{60} molecules, prompted by the first experiments of Martin *et al.* on positively charged clusters.[8] This mass spectroscopic study revealed magic numbers for clusters with less than 150 molecules that are indicative of structures based upon Mackay icosahedra.[9] The stability of the icosahedral $(C_{60})_{13}$ has since been further illustrated by Hansen *et al.*[10,11] However, subsequent calculations using the spherically averaged Girifalco potential[12] found that icosahedral structures are only lowest in energy up to $N=13$.[13–15] Above this size the structures are either decahedral or close packed. The rapid emergence of bulklike structures for this potential contrasts with many other atomic clusters where icosahedral structures can persist up to large sizes, for example, up to at least 20 000 atoms for sodium.[16] This behavior, and the marginal stability of the liquid phase, has a common origin in the narrowness of the C_{60} intermolecular potential well. As the range of a potential is decreased, there is an increasing energetic penalty for strained structures, be they icosahedra[17] or liquid configurations,[18,19] which involve nearest-neighbor distances that deviate from the equilibrium pair distance.

One possible cause of the discrepancy between experiment and theoretical calculations is the isotropic nature of the Girifalco potential. However, calculations using an all-atom model also found that icosahedra are only lowest in energy at small sizes, albeit to slightly larger sizes ($N=16$) than for the Girifalco potential.[20–22]

This situation led Shvartsburg and Jarrold to investigate the possibility of distinguishing icosahedral from decahedral and close-packed isomers by their mobility. However, the differences in the computed mobilities are small and were comparable to the experimental resolution.[23] More recently, Branz *et al.* performed some new mass spectroscopic experiments on $(C_{60})_N$ clusters to try to obtain further insights into the difference between theory and experiment.[24] They found that the observed structures are independent of the sign and magnitude of the charge. However, temperature was found to be a key variable in determining the structure. The initial cold as-grown clusters showed no magic numbers. Only on annealing at higher temperatures are the magic numbers revealed, as the relative evaporation rates cause larger populations to develop in those clusters that are more resistant to evaporation. After annealing at 490 K, as in the previous experiment, magic numbers consistent with icosahedral clusters are obtained. However, annealing at 585 K reveals a new set of magic numbers that correspond to non-icosahedral clusters.[25] As well as sizes associated with face-centered-cubic (fcc) and decahedral packing, particularly prominent were magic numbers associated with the recently discovered Leary tetrahedron.[26]

There are two possible explanations for this temperature dependence. First, the results could reflect changes in the thermodynamically most stable structures with temperature. Such solid-solid transitions have now been observed in a variety of systems.[17,27–33] However, for all these examples icosahedral structures are more stable at higher temperature,

and are favored because they have a larger vibrational entropy.[32] Furthermore, the theoretical calculations for $(C_{60})_N$ suggest that the non-icosahedral structures are lowest in energy and so would be favored at low temperature. Indeed, such a transition to a high-temperature icosahedral structure has been located for $(C_{60})_{14}$ interacting with the Girifalco potential[33] and has also been suggested for some larger clusters.[34] As the behavior of these solid-solid transitions is opposite to that of the experiment, this explanation is unlikely.

Secondly, the icosahedral structures could be more accessible during the growth and annealing of the clusters, with escape from the icosahedral region of configuration space into the state with lowest free energy only being possible at the highest temperatures. This interpretation has support from a variety of sources. For example, it has been shown that it is possible, under certain conditions, to preferentially grow metastable icosahedral clusters for silver.[35] Furthermore, analyses of the potential energy surface (PES) topography of those Lennard-Jones clusters with non-icosahedral global minima has shown that large energy barriers exist for interconversion of the icosahedral isomers and the global minimum, and that the icosahedral funnel is much wider.[36] Thus, on relaxation down the PES, the system is likely to become trapped in the icosahedral region of configuration space. This trapping is partly due to the greater structural similarity to the polytetrahedral configurations typical of the liquid, but also to the general energetic preference that Lennard-Jones clusters have for icosahedral geometries.[37] The latter would not hold for clusters of C_{60} molecules. Finally, short-ranged potentials have been shown to lead to relatively large barriers[38,39] and consequently to much slower dynamics.[40] Therefore, it is plausible that kinetic effects could dominate for $(C_{60})_N$ clusters on the experimental time scales, even for the relatively small clusters studied.

Many of the studies of the condensed-phase properties of C_{60} have used the Girifalco potential.[1,3–5,13–15,41] However, a new single-site potential has recently been derived by Pacheco and Prates-Ramalho (PPR) that gives an improved description of many properties of bulk C_{60}, including, for example, the dependence of the density of the crystal on pressure.[42] Furthermore, the high-temperature thermodynamics of clusters interacting with this potential are in reasonable agreement with those of an all-atom potential.[43] Here, we see if this potential can help to explain the experimental observations of Branz *et al.*[24] Global optimization has been previously attempted for the PPR potential.[34,44] However, the conclusions of these papers are contradictory and, as we shall see, many of the putative global minima are suboptimal. Here, as well as locating putative global minima for this potential, we also consider the most stable growth sequence for structures based on the experimentally observed Leary tetrahedra, and examine the PES topography and the thermodynamics of two example clusters.

II. METHODS

The PPR potential consists of a pair potential plus a three-body term of the standard Axilrod-Teller form.[45] The potential energy of the cluster is therefore given by

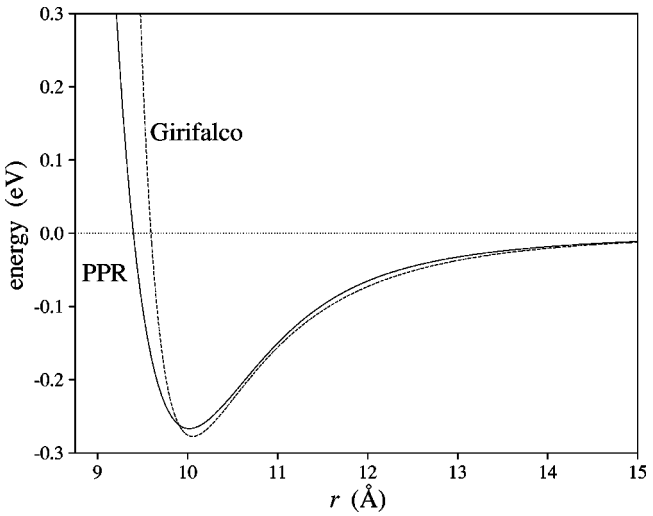

FIG. 1. Comparison of the PPR and Girifalco pair potentials.

$$E=\sum_{i<j} V_{\mathrm{pair}}(r_{ij})+C_{\mathrm{AT}}\sum_{i<j<k} V_{\mathrm{AT}}(r_{ij},r_{ik},r_{jk}), \qquad (1)$$

where C_{AT} gives the magnitude of the Axilrod-Teller term. The pair potential consists of a Morse form for the short-range repulsion, a van der Waals expansion for the long-range attraction and a Fermi function to describe the crossover between these two regimes. The forms of these functions and the associated parameters are given in Ref. 42.

As one can see from Fig. 1, the PPR pair potential has a softer repulsion than the Girifalco potential, leading to a wider potential well. This effect can be quantified by matching the second derivative at the bottom of the well to that of the Morse potential

$$V_M(r)=\epsilon\exp[\rho(1-r/r_{\mathrm{eq}})]\{\exp[\rho(1-r/r_{\mathrm{eq}})]-2\}, \quad (2)$$

where ϵ is the pair well depth and r_{eq} is the equilibrium pair distance. The Morse potential becomes increasingly narrow as the parameter ρ increases. The curvature at the bottom of the Morse well is $2\rho^2$ when the units of energy and distance are the pair well depth and equilibrium pair distance. This result can then be used to obtain a value of ρ_{eff}, a measure of the effective range, for each potential. This analysis has been done previously for the Girifalco potential leading to $\rho_{\mathrm{eff}}^{\mathrm{G}}=13.62$.[46] For the PPR potential, however, $\rho_{\mathrm{eff}}^{\mathrm{PPR}}=11.28$. This difference in ρ_{eff} has a well-understood effect on the resulting properties of the liquid[18,19,47] and of clusters.[17,48] For example, it will make the bulk PPR liquid phase more stable, as has been observed.[6] More importantly for this study, it will make icosahedral structures more stable than for the Girifalco potential.

The three-body Axilrod-Teller term always gives rise to a positive contribution to the energy for a compact structure. For example, its inclusion leads to a 6% increase in the energy of the bulk C_{60} crystal.[42] However, in the global optimization study of Ref. 44, the supposed global minima for the full PPR potential had a lower potential energy than those

when only the pair potential was used. This is clearly wrong and must have been due to some kind of error in the computation of the Axilrod-Teller term. Furthermore, in the other optimization study of PPR clusters, putative global minima were only located for the pair potential, because of the greater computational cost of the three-body term.[34]

The most unfavorable common configuration for the three-body Axilrod-Teller term is three nearest-neighbor molecules arranged in an equilateral triangle.[49] Therefore, one would expect the three-body energy to be larger for those structures that have more nearest neighbors, more polytetrahedral character and close-packed surfaces. Thus the Axilrod-Teller term disfavors icosahedral structures the most.[50]

To locate the global minima for the PPR potential we used basin hopping[51] (Monte Carlo plus minimization[52]), which has proved to be a very effective method for a variety of cluster systems. This approach[51,53] and the reasons for its success[27,54,55] have been described in detail elsewhere. The only specific modification for the present application was to reduce the computational cost of the minimizations by only switching on the three-body interactions close to convergence. Such a ''guiding function'' approach has previously been suggested and exploited by Hartke.[56] As well as basin hopping, we also reoptimized a large database of minima that we had obtained from previous optimization studies on Lennard-Jones,[51] Morse,[17,48] and Girifalco[15] clusters. Most of the global minima that we located were contained within this database.

To generate the samples of minima from which the disconnectivity graphs and the thermodynamics in Sec. IV were calculated, we used the same methods as those we have previously applied to LJ (Refs. 30,36,57) and Morse[39] clusters. We thereby obtain large samples of connected minima and transition states that provide good representations of the low-energy regions of the PES. The approach involves repeated applications of eigenvector following[58] to find new transition states and the minima they connect, as described in detail elsewhere.[59]

III. GLOBAL MINIMA

Putative global minima were located for the full PPR potential up to $N=105$, the size range of interest for comparison with the high temperature experiments of Branz *et al.*[24] The energies and point groups of these structures are given in Table I and coordinates are available on the world-wide web from the Cambridge Cluster Database.[60]

As expected, the energies of the global minima differ from those reported in Ref. 44, because of the error in the Axilrod-Teller term. To facilitate comparisons with the other results in Refs. 34 and 44, we also report the energies of these global minima when reoptimized for the PPR pair potential (Table I). The resulting energies will not necessarily be the global optima for the pair potential, but they should provide a good upper bound. Comparisons with these energies show that the putative global minima for the PPR pair potential given in Ref. 44 are suboptimal for $N \geqslant 19$ and those in Ref. 34 are suboptimal for $N=18$, 26, 33–36 and $N \geqslant 40$. Only for $N=16$ and 29 are lower two-body energies obtained in these papers,[34,44] indicating that for these cluster sizes the introduction of the Axilrod-Teller term leads to a change in the structure of the global minimum. For $N=16$ the relevant minimum is icosahedral with $E=-13.006550$ eV and $E_2=-13.447202$ eV, and for $N=29$ it is an alternative decahedral minimum with $E=-27.540094$ eV and $E_2=-28.516282$ eV.

In Fig. 2(a) we plot the energies of the PPR global minima so that particularly stable clusters stand out. We also provide a comparison with results for the Girifalco potential [Fig. 2(b)], partly because a significant number of the putative global minima in Ref. 15 have now been improved (an up-to-date list is maintained at the Cambridge Cluster Database[60]). A selection of the global minima are depicted in Fig. 3.

At $N=13$ the icosahedral global minimum is noticeably more stable than for the Girifalco potential, which is consistent with the PPR potential's slightly wider well. Furthermore, icosahedral structures are lowest in energy up to 15 molecules, or up to 16 molecules if the Axilrod-Teller term in the potential is not included—as noted in Sec. II this term slightly disfavors icosahedral structures. However, contrary to the claims of Refs. 34 and 44 there are no further icosahedral global minimum above this size. Instead decahedral or close-packed clusters are lowest in energy.

To illustrate how the relative stabilities of icosahedral structures with respect to the global minimum evolve with size, we give the energy differences for examples where particularly stable fcc and icosahedral forms are available. At $N=38$ the difference in energy between the fcc truncated octahedron and the lowest-energy icosahedral structure is 0.582 eV. However, at $N=55$ the Mackay icosahedron is 0.297 eV above the decahedral global minimum. When the Axilrod-Teller interactions are not included this difference decreases to 0.159 eV, again illustrating that this term slightly disfavors icosahedra. In contrast, the energy difference for the Girifalco potential is a considerably larger 1.997 eV. These results are consistent with the behavior expected from the respective values of ρ_{eff}: the Mackay icosahedron is lowest in energy for the Morse potential up to $\rho=11.15$ and then becomes increasingly unstable as the width of the potential decreases further.

The pronounced minima in Fig. 2 correspond to particularly low-energy structures that could potentially give rise to magic numbers. Comparing (a) and (b) of Fig. 2 it is apparent that the patterns are very similar, indicating that the two C_{60} potentials favor similar structures. Prominent in both figures are the same particularly stable decahedral and close-packed forms, most of which are illustrated in Fig. 3. The main differences are that, for the Girifalco potential, the feature due to $(C_{60})_{13}$ is much less pronounced, for the reasons explained above, and that the close-packed structures are somewhat more favored. The latter feature is again due to the shorter range of the Girifalco potential, as is the greater number of close-packed global minima for the Girifalco potential.

There is some correspondence between Fig. 2 and the high temperature magic numbers observed experimentally.[24]

TABLE I. Energies and point groups for the putative global minima for $(C_{60})_N$ clusters modeled by the PPR potential. The energies of these minima when reoptimized without the inclusion of the three-body term (E_2) are also given. Structural assignments are given for all clusters with $N \geqslant 13$, where *i* stands for icosahedral, *d* for decahedral (d^+ have an overlayer on the {111} faces), *f* for fcc, and *c* for close packed (but not fcc). Fcc and close-packed structures can be unstrained.

N	PG	S	*E*/eV	E_2/eV	*N*	PG	S	*E*/eV	E_2/eV	*N*	PG	S	*E*/eV	E_2/eV
3	D_{3h}		-0.793763	-0.800181	38	O_h	*f*	-38.726684	-40.164289	73	C_s	*d*	-82.892601	-86.232181
4	T_d		-1.574722	-1.600362	39	C_{4v}	*f*	-39.803068	-41.276819	74	C_{5v}	*d*	-84.275939	-87.683469
5	D_{3h}		-2.360685	-2.406624	40	C_{2v}	*f*	-40.879585	-42.389454	75	D_{5h}	*d*	-85.854200	-89.335316
6	O_h		-3.179823	-3.251103	41	C_{2v}	*d*	-42.050754	-43.620062	76	C_s	*d*	-86.943730	-90.469387
7	D_{5h}		-4.174831	-4.277606	42	C_s	*d*	-43.134640	-44.743772	77	C_{2v}	*d*	-88.287170	-91.870873
8	C_s		-4.971222	-5.095539	43	C_{2v}	*d*	-44.465028	-46.115661	78	C_1	*d*	-89.376306	-93.004550
9	C_{2v}		-5.979744	-6.139683	44	C_s	*d*	-45.548888	-47.250124	79	D_{3h}	*c*	-90.750950	-94.414956
10	C_{3v}		-6.941044	-7.136890	45	C_{2v}	*d*	-46.879111	-48.632640	80	C_s	*c*	-91.847206	-95.555790
11	C_{2v}		-7.890403	-8.122285	46	C_s	*c*	-47.964493	-49.771293	81	C_{2v}	*c*	-93.195399	-96.961852
12	C_{5v}		-8.910974	-9.191726	47	C_{2v}	*d*	-49.293304	-51.138897	82	C_{2v}	*d*	-94.475899	-98.305791
13	I_h	*i*	-10.203987	-10.556666	48	C_{2v}	d^+	-50.835900	-52.786358	83	C_{2v}	*c*	-95.639897	-99.508789
14	C_{3v}	*i*	-11.010918	-11.384715	49	C_s	d^+	-51.926724	-53.919060	84	C_{2v}	*d*	-96.907100	-100.839577
15	C_{2v}	*i*	-12.028948	-12.436957	50	D_{3h}	*c*	-53.354529	-55.400213	85	C_{3v}	*c*	-98.138499	-102.126340
16	C_{2v}	*d*	-13.017348	-13.429036	51	C_s	*c*	-54.449934	-56.540311	86	C_{3v}	*c*	-99.728365	-103.787568
17	C_{2v}	*d*	-14.088380	-14.538481	52	C_{2v}	*c*	-55.797330	-57.945711	87	C_s	*c*	-100.867536	-104.983413
18	D_{5h}	*d*	-15.163644	-15.653781	53	C_s	*c*	-56.892907	-59.085964	88	C_s	*c*	-102.173549	-106.335126
19	C_{2v}	*d*	-16.218799	-16.743185	54	C_{2v}	*d*	-58.306782	-60.570092	89	C_s	d^+	-103.461268	-107.695215
20	C_{2v}	*d*	-17.274543	-17.832640	55	C_{2v}	*d*	-59.408665	-61.716335	90	C_s	d^+	-104.807341	-109.095407
21	C_s	d^+	-18.353074	-18.949300	56	C_s	*d*	-60.752438	-63.116143	91	C_{3v}	*c*	-106.302975	-110.678677
22	C_1	d^+	-19.425310	-20.059762	57	C_{2v}	*d*	-62.098302	-64.517510	92	C_s	*c*	-107.397152	-111.806846
23	C_s	d^+	-20.686563	-21.386861	58	D_{3h}	d^+	-63.386632	-65.901565	93	C_s	*c*	-108.747951	-113.216329
24	C_1	d^+	-21.759634	-22.497858	59	T_d	*c*	-64.769800	-67.323349	94	C_s	*c*	-110.100130	-114.626428
25	C_{3v}	d^+	-22.957151	-23.760958	60	C_s	*d*	-65.887129	-68.480038	95	C_{2v}	*d*	-111.653413	-116.285755
26	C_{2v}	d^+	-24.141029	-24.968567	61	C_{3v}	*f*	-67.169082	-69.798058	96	C_s	*d*	-112.771588	-117.460346
27	C_s	d^+	-25.218788	-26.085977	62	C_1	*d*	-68.330220	-71.021579	97	C_1	*d*	-114.123353	-118.862596
28	C_s	d^+	-26.403185	-27.334120	63	C_s	*d*	-69.702863	-72.458970	98	C_s	*c*	-115.518307	-120.295415
29	D_{5h}	*d*	-27.542310	-28.503488	64	C_{2v}	*d*	-71.278073	-74.107991	99	C_s	*d*	-117.079750	-121.959509
30	C_{2v}	d^+	-28.649061	-29.682832	65	C_{2v}	*d*	-72.382930	-75.268852	100	T_d	*c*	-118.491490	-123.409546
31	C_{2v}	*d*	-29.963558	-31.028821	66	C_s	*d*	-73.720048	-76.664850	101	D_{5h}	*d*	-120.052347	-125.073354
32	C_1	*d*	-31.047706	-32.157893	67	C_{2v}	*d*	-75.059516	-78.062777	102	C_{2v}	*d*	-121.170243	-126.247600
33	C_{2v}	*d*	-32.386698	-33.555532	68	C_1	*d*	-76.157881	-79.200432	103	C_s	*d*	-122.516174	-127.652314
34	C_1	*d*	-33.469737	-34.683456	69	C_1	*d*	-77.504125	-80.605732	104	C_{2v}	*d*	-123.864106	-129.058381
35	C_{2v}	*d*	-34.807885	-36.080228	70	C_s	*d*	-78.872607	-82.039199	105	C_s	*d*	-124.981491	-130.232109
36	C_1	*d*	-35.889548	-37.206754	71	C_{2v}	*d*	-80.450302	-83.690481					
37	C_{2v}	*d*	-37.226573	-38.602386	72	C_1	*d*	-81.545223	-84.828030					

Small peaks in the mass spectrum at $N=31$, 33, and 35 probably correspond to a series of small decahedra. Similarly, the peak at $N=38$ can be assigned to the fcc truncated octahedron, and the peaks at $N=64$, 71 and 75 are probably due to Marks decahedra. Particularly interesting is the feature in Fig. 2 corresponding to the decahedral $(C_{60})_{48}$ global minimum, because the most prominent peak in the mass spectrum occurs at $N=48$. As with a number of the other decahedral global minima (Table I), this structure has an overlayer on the {111} faces in sites which are hcp with respect to the five slightly strained fcc tetrahedra that are the basis of decahedral structures. In fact, many of these structures are fragments of larger Mackay icosahedra with the apex of the decahedron corresponding to what would become the center of the icosahedron. Indeed, growth simulations for silver have indicated that the addition of this overlayer does provide a natural pathway to the growth of larger icosahedra.[35]

However, many of the particularly stable structures, especially for $N \geqslant 50$, do not correspond to magic numbers in the experiment. There are no experimental peaks corresponding to the close-packed tetrahedra at $N=59$ and 100, nor to the twinned truncated octahedra at $N=50$ and 79 and the 101-molecule Marks decahedron. Instead, peaks occur in the mass spectrum at $N=58$, 61, 68, 77, 84, 91, 96, and 98, which cannot be simply explained by reference to the global minima of model C_{60} potentials. These peaks have previously been assigned[24] to structures based on a 98-molecule Leary tetrahedron.[26] This recently discovered structure is illustrated in Fig. 4. It can be described in terms of five fcc tetrahedra arranged into a stellated tetrahedron with apex

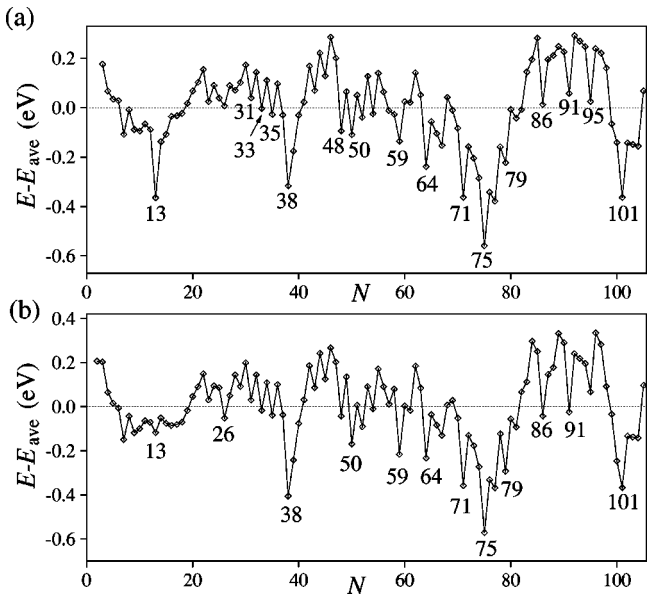

FIG. 2. Energies of the global minima for $(C_{60})_N$ clusters modeled by the (a) PPR and (b) Girifalco potentials. The energy zero is taken to be E_{ave}, a four-parameter fit to the energies of the global minima. For the PPR potential $E_{ave}/\text{eV} = -1.6537N + 2.1901N^{2/3} + 0.1263N^{1/3} - 0.7467$. For the Girifalco potential $E_{ave}/\text{eV} = -1.789N + 2.294N^{2/3} + 0.5907N^{1/3} - 1.292$.

molecules removed and seven-molecule hexagonal patches covering the edges of the central tetrahedron. That this structure is not the global minimum for the PPR or Girifalco potential is consistent with the values of ρ_{eff}. For the Morse potential it is only the global minimum for $6.91 < \rho < 9.45$ because it has a strain energy intermediate between decahedra and icosahedra.

To attempt to add further weight to the experimental assignments we calculated the energies of a series of structures derived from the Leary tetrahedron. Although they are not lowest in energy, the size variation of their energies, plotted for $60 < N < 100$ in Fig. 5, is insightful. There is remarkable agreement between the features in this graph and the remaining magic numbers.

The stable structures for the Leary tetrahedral growth sequence are illustrated in Fig. 4. The 91-molecule structure is derived by removing a hexagonal patch from over one of the edges of the central tetrahedron. In contrast, to obtain the 89-molecule structure one of the points of the Leary tetrahedron is further truncated. By a similar truncation the $(C_{60})_{91}$ global minimum can be derived from the 100-molecule tetrahedral global minimum (Fig. 3). Most of the other structures can be obtained by a combination of these two changes. The 84-molecule structure is derived by a truncation and the removal of an adjacent patch. Similarly, truncation of two of the fcc tetrahedra and the removal of the common patch gives the 77-molecule structure. The 68-molecule structure is derived by completely removing one of the fcc tetrahedra and adjacent patches, thus giving a structure that is also a fragment of the 147-molecule Mackay icosahedron. The truncation of a further tetrahedron leads to the 61-molecule structure.

Interestingly, the latter two structures are global minima for Morse clusters, but were not located in the most recent optimization study.[48] They have energies of $E_{61}(\rho = 10) = -252.488332\epsilon$ and $E_{68}(\rho = 10) = -286.643320\epsilon$, and are lowest in energy in the ranges $9.42 < \rho < 10.34$ and $7.40 < \rho < 11.55$, respectively.

The prominence of the peak in the mass spectrum at $N = 48$ also fits with this preference for structures based upon the Leary tetrahedron. The second view of the decahedral $(C_{60})_{48}$ global minimum in Fig. 3 shows that it is also a fragment of the Leary tetrahedron. By adding an identical overlayer to the bottom {111} faces of this cluster the decahedral $(C_{60})_{58}$ global minimum is obtained, which is again a fragment of the Leary tetrahedron. Although this cluster is not especially stable compared to nearby sizes for the PPR potential, its relationship to the Leary tetrahedron provides a basis for confidently assigning the remaining magic number at $N = 58$ to this structure.

IV. $(C_{60})_{38}$ AND $(C_{60})_{55}$

Although the location of the global minima should be the first step in the theoretical determination of a cluster's struc-

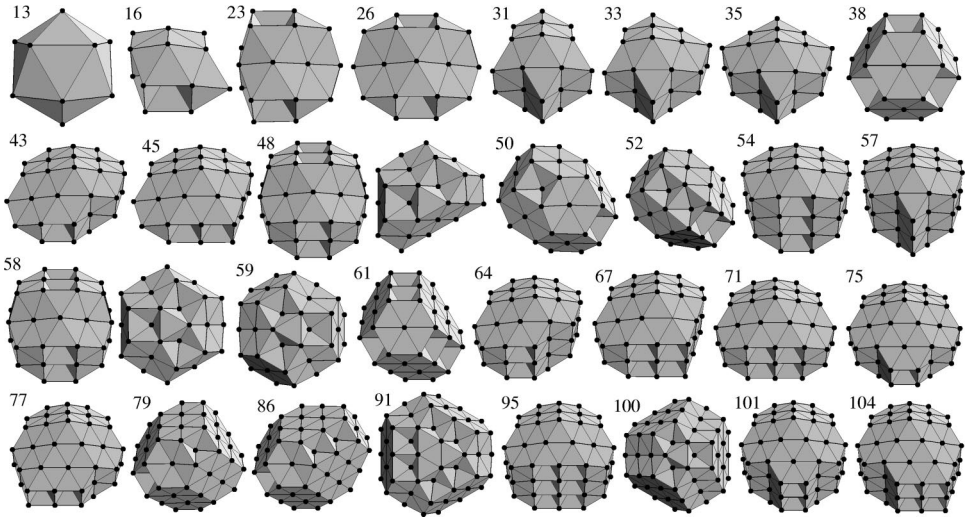

FIG. 3. A selection of the global minima for the PPR potential. Each C_{60} molecule is represented by a point at the molecular center. Structural assignments for each of the clusters are given in Table I. The two views of the 48- and 58-molecule clusters illustrate the relationship of these structures to both decahedra and the Leary tetrahedron.

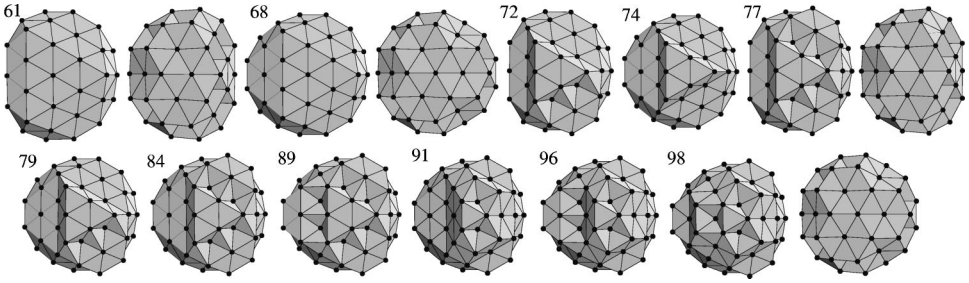

FIG. 4. Particularly stable clusters on the growth sequence leading to the Leary tetrahedron. When two viewpoints are given they correspond to the front and back of the cluster.

ture, the thermodynamics[32] and dynamics[61] can also play an important role. Here, we examine the behavior of two example clusters in more detail. We choose $(C_{60})_{38}$ and $(C_{60})_{55}$ because particularly stable fcc (38) and icosahedral (55) structures are possible. Furthermore, these sizes have been extensively studied for the longer-ranged Lennard-Jones potential.[27,30,36,40,62,63]

In order to construct disconnectivity graphs for these two clusters we have generated large samples of minima and transition states, plus the pathways connecting them. As this is a computationally demanding task only the two-body component of the PPR potential was used. The graphs for the full potential would be very similar; the main effect of the introduction of the three-body term would be to displace the icosahedral regions of configuration space further up in energy. We located 38 558 minima and 39 959 transition states for $N=38$ and 39 043 minima and 39 846 transition states for $N=55$.

Disconnectivity graphs[64,65] provide a representation of the barriers between minima on a PES.[64,65] In a disconnectivity graph, each line ends at the energy of a minimum. At a series of equally spaced energy levels we determine which (sets of) minima are connected by paths that never exceed that energy. We then join up the lines in the disconnectivity graph at the energy level where the corresponding (sets of) minima first become connected. In a disconnectivity graph an ideal single-funnel[66,67] PES would be represented by a single dominant stem associated with the global minimum to which the other minima directly join. For a multiple-funnel PES there would be a number of major stems that only join at high energy. A single funnel PES is typically associated with efficient relaxation to the global minimum, whereas for a multiple-funnel PES there is a separation of time scales between relaxation to a low-energy structure and interfunnel equilibrium.[59]

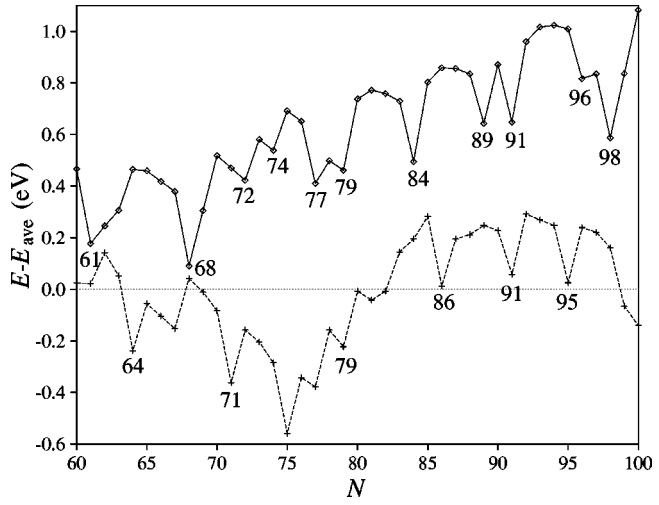

FIG. 5. Energies of structures based upon the 98-molecule Leary tetrahedron (solid line) compared to the energies of the global minima (dashed line) for the PPR potential.

For $(C_{60})_{38}$ and $(C_{60})_{55}$ it is not possible to characterize the whole PES because of the huge numbers of minima. In addition, even if we could perform such a characterization, any attempt at representation using a disconnectivity graph would just be obscured by the density of lines. Therefore, we concentrate on the low-energy regions of the PES that are of most importance when considering structure, and only include the lines leading to the lowest 250 minima.

For both clusters the PES topography has a multiple-funnel character, where each funnel corresponds to a different structural type (Fig. 6). For this short-ranged potential, there are a number of competing low-energy morphologies that are separated by large energetic barriers. As the barriers between minima of the same structural type are typically much smaller, the graphs clearly separate the different morphologies.

This behavior contrasts with that for Lennard-Jones clusters, which (with some notable exceptions) typically have a single-funnel topography that is dominated by icosahedral structures.[36] However, for the PPR potential the difference in energy between close-packed and decahedral structures is small. Furthermore, there are often a number of close-packed forms possible that have significant structural differences. For example, for $(C_{60})_{55}$ the close-packed region of configuration space divides up into structures that are based on the 50-molecule global minimum (the twinned truncated octahedron) and those based on the 59-molecule tetrahedral global minimum (Fig. 3). Additionally, as well as a funnel leading to the conventional decahedral global minimum, there is a low-energy region of configuration space corresponding to decahedral structures that have the {111} faces partially covered. These latter structures can be constructed by adding molecules to the 48-molecule global minimum. This complexity of the $(C_{60})_{55}$ disconnectivity graph contrasts with that of $(C_{60})_{38}$, for which there are only funnels associated with the three basic morphologies.

The disconnectivity graphs can tell us a lot about the dynamics of these two clusters. On the disconnectivity graphs we give the numbers of minima in our sample that are associated with each funnel. Although these are large underestimates of the true values because of the incompleteness of our

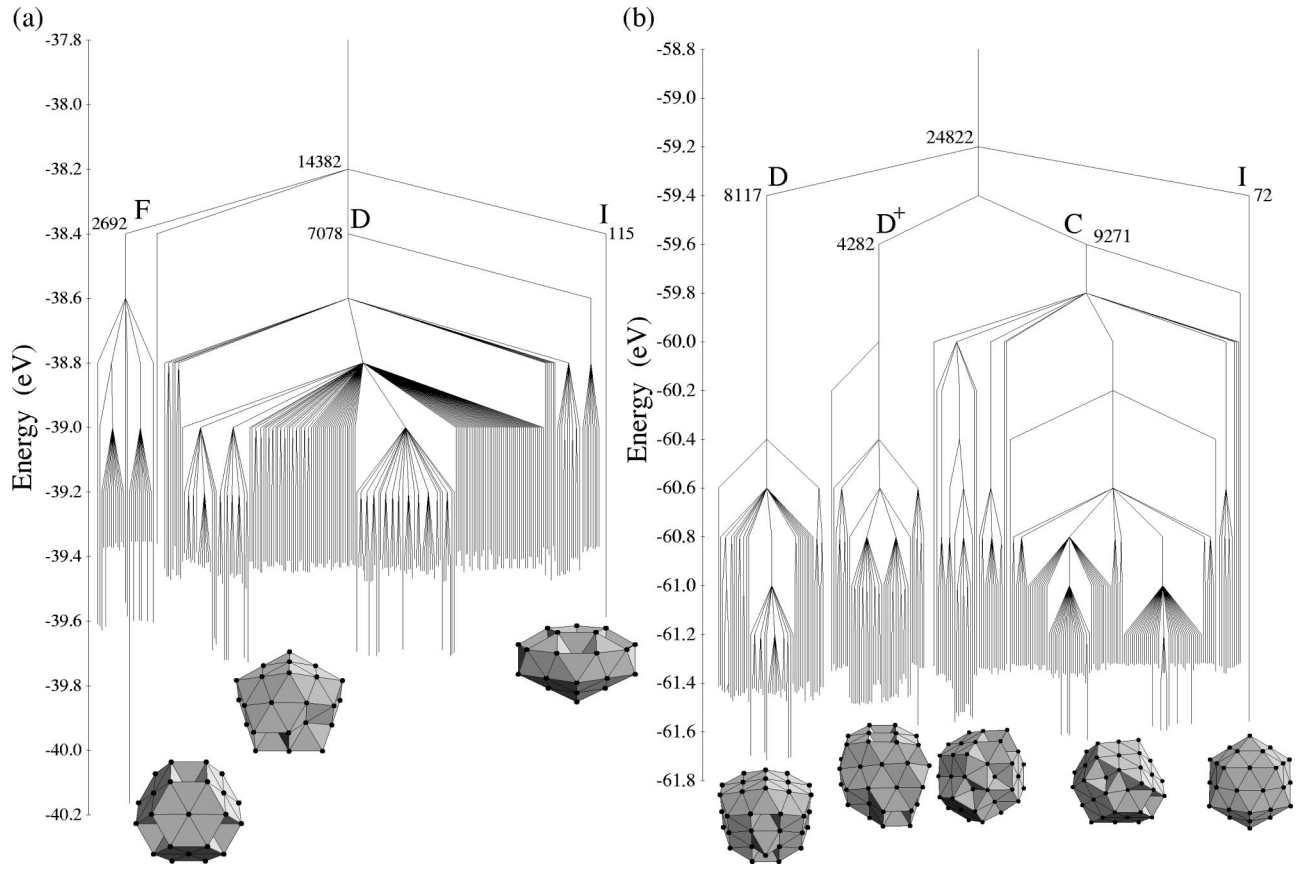

FIG. 6. Disconnectivity graphs for (a) $(C_{60})_{38}$ and (b) $(C_{60})_{55}$. Lines corresponding to the lowest 250 minima are represented. Structural labels have been placed adjacent to the lines corresponding to the different funnels on the PES, where, as in Table I, *I* stands for icosahedral, *D* for decahedral (D^+ have an overlayer on the {111} faces), *F* for fcc, and *C* for close packed. The numbers refer to the number of minima below the corresponding node in the full graph. Pictures of the lowest-energy minima for the different structural types have been placed adjacent to the corresponding lines.

samples, they do provide a reasonable indication of the relative numbers of low-energy minima of each structural type, and hence of the widths of the funnels in configurational terms. It is particularly noticeable that there are far fewer low-energy icosahedral minima, as expected for a short-ranged potential. By contrast, the number of decahedral and close-packed structures is of the same order.

Based on this information, on relaxation down the PES one would expect the system to be more likely to end up in a close-packed or decahedral configuration. However, there are other factors that can influence the dynamical behavior. There is a vibrational, as well as a configurational, contribution to the width of a funnel. This term is larger for the icosahedral funnel because the associated minima are generally flatter and wider. Furthermore, it may also be that the icosahedral structures lie, in some sense, closer to the liquidlike region of configuration space because of their greater polytetrahedral character.[19,68]

Structure formation in clusters does not necessarily occur by relaxation from a high-energy state, but can also occur by growth from a smaller preexisting solid cluster.[61] Although the width of the funnels is less important in this case, the disconnectivity graphs can still be useful because they give an idea of the kinetic stability of the possible structures. The large barriers between funnels suggest that, except at high temperature, trapping will occur within the funnel of the existing structure, even if the structure is metastable. Indeed escape from a funnel will become more difficult with increasing size because the interfunnel barriers become larger.

Therefore, during cluster growth, except at high temperatures and extremely long time scales, the smaller clusters serves as templates for growth and only the optimization of the position of additional loosely bound molecules is likely to occur. If icosahedral structures are preferred at the last size for which equilibrium is possible, then larger icosahedra will result. Thus, the disconnectivity graphs give additional support to the idea that icosahedra are observed experimentally because of kinetic trapping at low temperature.

To examine the low-temperature thermodynamics of the two clusters in question we use the harmonic superposition method.[59,69] In this approach the partition function is constructed by summing the partition functions of the individual minima on the PES. In the harmonic approximation, we obtain

$$Z = \sum_i \frac{n_i \exp(-\beta E_i)}{(\beta h \bar{\nu}_i)^{3N-6}}, \tag{3}$$

where E_i is the energy of minimum i, $\bar{\nu}_i$ is the geometric mean frequency and n_i is the number of permutational iso-

mers ($2N!/h_i$, where h_i is the order of the point group).

This approach is unable to reproduce high temperature behavior such as melting in the present cases, because no effort has been made to compensate for the incompleteness of our samples of minima, thus leading to an underestimate of the configurational entropy of the high-energy states. It is possible to overcome this limitation by using information obtained from an ergodic simulation,[59,69] but this is not attempted because ergodicity is hard to achieve for these clusters and because we are more interested in solid-solid transitions, for which we only need to characterize the low-energy regions of the PES. Instead we used parallel tempering to locate the point at which the cluster melts or boils. It is also possible to introduce anharmonicity into this scheme,[70,71] however, this additional level of complexity is unnecessary for the insights we are seeking to achieve here.

The advantage of the superposition method is the ease with which the low-temperature thermodynamics can be obtained even when, as with $(C_{60})_N$ clusters, there are large interfunnel energy barriers present. In fact it is not clear if any other method would be able to probe this regime, because of the difficulty of achieving ergodicity. Even techniques based on parallel tempering,[72,73] which are the only direct simulation methods that have been shown to succeed for challenging cases involving low-temperature solid-solid transitions in clusters,[31,74] failed for $(C_{60})_{55}$. The success of these methods relies on the coupling of the low-temperature runs to ergodic high-temperature runs involving molten clusters. However, because of the narrowness of any range of stability for the liquid-like state of clusters of C_{60} molecules[41,43] this is very hard to achieve.

Heat capacity curves for the two clusters are presented in Fig. 7. These were calculated using the same samples of minima as for the disconnectivity graphs. It was also possible to reoptimize all the minima for the full potential. Both clusters show some evidence of solid-solid transitions.

For $(C_{60})_{55}$ the energy gap between the icosahedral minima and the global minimum is relatively small and so a transition to the Mackay icosahedron occurs significantly below the melting temperature. For the full potential this transition occurs at 377 K and, consistent with the reduction in the energy gap, at 184 K when the three-body term is neglected. Interestingly, there is also a small peak at ~ 45 K, which corresponds to a redistribution of the equilibrium occupation probability amongst the five lowest-energy decahedral isomers. These minima are almost isoenergetic and correspond to the five different positions that the four-coordinate surface molecule can occupy. The high-temperature peak corresponds to the beginnings of the melting/boiling transition, which as expected is underestimated by the harmonic superposition method. Parallel tempering indicates that the actual peak for this transition is much larger and occurs at ~ 950 K, although the result is somewhat dependent on the size of the constraining box in which the cluster is placed.

For $(C_{60})_{38}$ the calculated heat capacity curve is much simpler and only has a single peak. This corresponds to the transition out of the truncated octahedron, first roughly equally into the low-energy decahedral minima and lowest-energy icosahedral minimum, and then at slightly higher temperature into the higher-energy states. As these transitions are so close together in temperature there is only a single peak in the heat capacity, which is centered on the initial transition because of the underestimation of the latent heat of melting by the present approach. Parallel tempering simulations suggest that the preliminary solid-solid transition gives rise to a shoulder in the melting peak, which occurs at ~ 900 K.

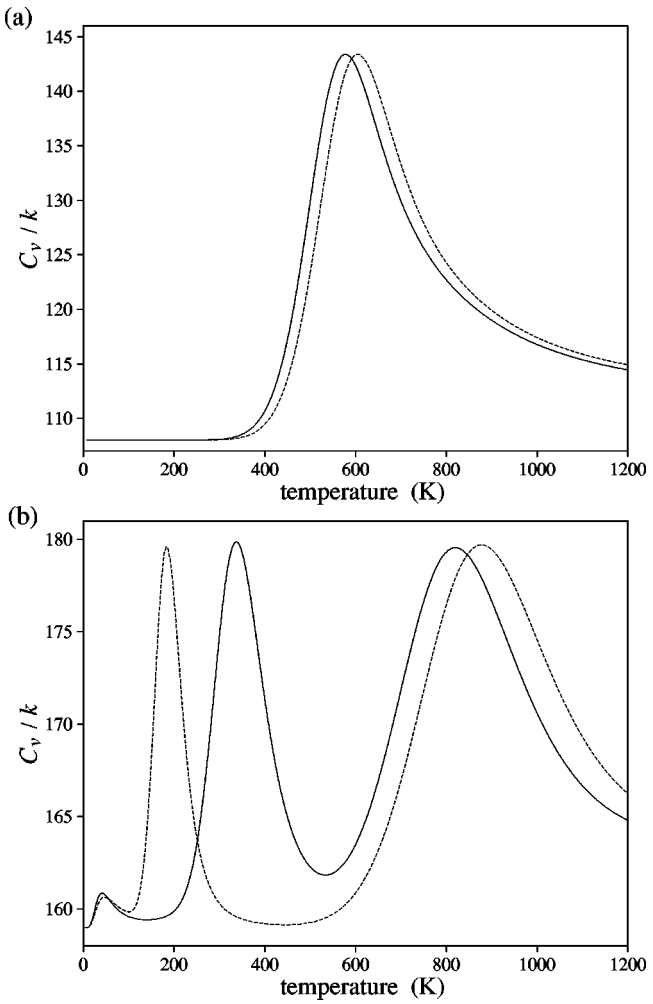

FIG. 7. Heat capacity curves for (a) $(C_{60})_{38}$ and $(C_{60})_{55}$ obtained from our samples of minima using the harmonic superposition method. The solid lines are for the full potential and the dashed lines are for the two-body potential.

As for the solid-solid transitions that have been investigated in detail for Lennard-Jones clusters,[32,75] the above transitions are driven by the larger vibrational entropy of the icosahedral structures. However, the differences in the vibrational frequencies for the current system are significantly larger. For $N=38$ $\bar{\nu}_{\rm icos}:\bar{\nu}_{\rm deca}:\bar{\nu}_{\rm cp}=0.920:0.977:1$ and for $N=55$ 0.909:1:0.999, where we have used the values for the lowest-energy minimum of each structural type. These properties reflect the general trends for the vibrational frequencies to be lower for more strained structures, and for the differences to increase as the potential becomes more short ranged.[75]

Although we have only considered two sizes in detail, the large temperature window for which the Mackay icosahedron is most stable indicates that solid-solid transitions are likely to be common for other sizes. The results confirm what has been emphasized elsewhere, namely, that crossover sizes at which the dominant structure changes depend on temperature.[32] So, although none of the clusters above $N=15$ have icosahedral global minima, icosahedra can still be thermodynamically most stable for some range of temperature above this size. For example, similar calculations indicate that for $(C_{60})_{19}$ icosahedral structures are favored above 333 K. However, these results cannot explain the experimental observation of icosahedra, because they are seen below, not above, a transition temperature.

We can also use the current methods to examine whether the Leary tetrahedron might be stabilized at high temperature. As Leary tetrahedra have a strain energy intermediate between icosahedra and decahedra, their mean vibrational frequency is lower than for decahedral and close packed clusters. For example, for $(C_{60})_{98}$ $\bar{\nu}_{\rm icos}:\bar{\nu}_{\rm Leary}:\bar{\nu}_{\rm deca}:\bar{\nu}_{\rm cp}=0.925:0.972:0.997:1$. Although the Leary tetrahedron does develop a small equilibrium population near to the melting point in the current model, there is no clear transition at which the Leary tetrahedron becomes the dominant structure.

V. CONCLUSIONS

Putative global minima for the C_{60} intermolecular potential of Pacheco and Prates-Ramalho have been located for all clusters containing up to 105 molecules. For $N\leqslant 15$ the structures follow an icosahedral growth sequence, but above this size the global minima are either decahedral or close packed, with close-packed clusters becoming more common as the size increases. This progression to structures with lower strain energy as the size increases is expected, but is more rapid than for most atomic clusters, because the PPR potential is much more short-ranged than typical interatomic potentials.

The correspondence between many of the particularly low-energy PPR clusters and the high-temperature experimental magic numbers adds further support to the interpretation that these sizes have particularly low free energies because they are particularly low in potential energy. This interpretation also implies that the icosahedral magic numbers seen at lower temperature are kinetic in origin. The large interfunnel barriers evident from the disconnectivity graphs of $(C_{60})_{38}$ and $(C_{60})_{55}$ add further support to this hypothesis by indicating the difficulty of major structural transformations in a growing cluster. Moreover, preliminary results from growth simulations confirm this scenario.[76]

However, there are still discrepancies between the high temperature magic numbers and the low-energy model C_{60} clusters. First, the magic number at $N=19$, which persists up to high temperature, is probably due to the double icosahedron. This perhaps suggests that the PPR potential is still effectively too short ranged, but an alternative explanation is the thermal stabilization of this structure at the experimental temperature.

Secondly, a particular preference for structures that are based on the Leary tetrahedron is not reproduced. It is possible that these structures are only lowest in free energy at high temperature, but this seems unlikely for two reasons. First, as the entropy is not so strongly size dependent as the energy, magic numbers associated with structures that are entropically preferred are likely to be less pronounced. However, in the present case the magic numbers associated with the structures based upon the Leary tetrahedron are the most prominent. Secondly, no such transition is seen for $(C_{60})_{98}$. Hence, it is more likely that the discrepancy is due to the potential, and again suggests that the PPR potential is effectively too short ranged. For the Morse potential the 98-atom Leary tetrahedron is lowest in energy for $6.91<\rho<9.45$. However, the situation is somewhat more complex. Only at a few sizes are structures based on the Leary tetrahedron actually the global minima of the Morse potential. Therefore, the observed preference cannot simply be explained by the effective range. It is most likely to be related to the orientational degrees of freedom that are neglected in a single-site potential, such as the PPR model.

The thermodynamics calculations also indicate further discrepancies between experiment and the PPR model. We saw in Sec. IV that icosahedral structures are thermodynamically favored at high temperature for certain sizes, because of their larger vibrational entropy. However, except perhaps for $N=19$, there is no experimental support for this scenario.

Although all-atom potentials have been employed for modeling clusters of (C_{60}) molecules,[20–22] the double icosahedron was found not to be lowest in energy for $N=19$ and the potentials were not applied in the size range relevant to structures based on the Leary tetrahedron. Furthermore, these types of all-atom potential are unable to reproduce the low-temperature properties of bulk C_{60}—the molecules have the incorrect orientation in the low-temperature crystal.[77] Although, at the temperatures relevant to experiment, the molecules are expected to be able to rotate freely,[78] it could well be that the energetic preferences for structures in which the molecules can have the preferred orientations will persist up to higher temperature. Therefore, to reproduce the preference for Leary tetrahedra it is likely that a potential that can give the correct orientations in the crystal is required. There are a number of such potentials,[79–81] however, this orientational preference has sometimes been achieved through the introduction of unrealistic electrostatic properties for the C_{60} molecule.[82] Still, it would be interesting to know if these potentials do favor Leary tetrahedra. However, this would be an extremely challenging task computationally, both because of the complexities of the potentials and the huge number of possible orientational isomers for such large clusters.

J.P.K.D. is grateful to Emmanuel College, Cambridge for financial support.

*Electronic address: jon@clust.ch.cam.ac.uk

[1] M. H. J. Hagen, E. J. Meijer, G. C. A. M. Mooij, D. Frenkel, and H. N. W. Lekkerkerker, Nature (London) **365**, 425 (1993).
[2] J. Q. Broughton, J. V. Lill, and J. K. Johnson, Phys. Rev. B **55**, 2808 (1997).
[3] A. Cheng, M. L. Klein, and C. Caccamo, Phys. Rev. Lett. **71**, 1200 (1993).
[4] C. Caccamo, D. Costa, and A. Fucile, J. Chem. Phys. **106**, 255 (1997).
[5] M. Hasegawa and K. Ohno, J. Chem. Phys. **111**, 5955 (1999).
[6] A. L. C. Ferreira, J. M. Pacheco, and J. P. Prates-Ramalho, J. Chem. Phys. **113**, 738 (2000).
[7] M. Hasegawa and K. Ohno, J. Chem. Phys. **113**, 4315 (2000).
[8] T. P. Martin, U. Mäher, H. Schaber, and U. Zimmermann, Phys. Rev. Lett. **70**, 3079 (1993).
[9] A. L. Mackay, Acta Crystallogr. **15**, 916 (1962).
[10] K. Hansen, H. Hohmann, R. Müller, and E. E. B. Campbell, J. Chem. Phys. **105**, 6088 (1996).
[11] K. Hansen, H. Hohmann, R. Müller, and E. E. B. Campbell, Z. Phys. D: At., Mol. Clusters **40**, 361 (1997).
[12] L. A. Girifalco, J. Phys. Chem. **96**, 858 (1992).
[13] C. Rey, L. J. Gallego, and J. A. Alonso, Phys. Rev. B **49**, 8491 (1994).
[14] D. J. Wales, J. Chem. Soc., Faraday Trans. **90**, 1061 (1994).
[15] J. P. K. Doye and D. J. Wales, Chem. Phys. Lett. **262**, 167 (1996).
[16] T. P. Martin, T. Bergmann, H. Göhlich, and T. Lange, Chem. Phys. Lett. **172**, 209 (1990).
[17] J. P. K. Doye, D. J. Wales, and R. S. Berry, J. Chem. Phys. **103**, 4234 (1995).
[18] J. P. K. Doye and D. J. Wales, Science **271**, 484 (1996).
[19] J. P. K. Doye and D. J. Wales, J. Phys. B **29**, 4859 (1996).
[20] C. Rey, J. Garcia-Rodeja, and L. J. Gallego, Z. Phys. D: At., Mol. Clusters **40**, 395 (1997).
[21] J. P. K. Doye, A. Dullweber, and D. J. Wales, Chem. Phys. Lett. **269**, 408 (1997).
[22] J. Garcia-Rodeja, C. Rey, and L. J. Gallego, Phys. Rev. B **56**, 6466 (1997).
[23] A. A. Shvartsburg and M. F. Jarrold, Chem. Phys. Lett. **86**, 261 (1996).
[24] W. Branz, N. Malinowski, H. Schaber, and T. P. Martin, Chem. Phys. Lett. **328**, 245 (2000).
[25] These temperatures are related to the time the clusters spend in the heating cell, which was approximately 0.5 ms (Ref. 24). If the heating time in the experiment is increased the temperatures for the observation of the icosahedral and non-icosahedral structures decrease somewhat. For example, for a heating time of 1 ms the decreases are 15–20 K.
[26] R. H. Leary and J. P. K. Doye, Phys. Rev. E **60**, R6320 (1999).
[27] J. P. K. Doye and D. J. Wales, Phys. Rev. Lett. **80**, 1357 (1998).
[28] C. L. Cleveland, W. D. Luedtke, and U. Landman, Phys. Rev. Lett. **81**, 2036 (1998).
[29] C. L. Cleveland, W. D. Luedtke, and U. Landman, Phys. Rev. B **60**, 5065 (1999).
[30] J. P. K. Doye, M. A. Miller, and D. J. Wales, J. Chem. Phys. **110**, 6896 (1999).
[31] J. P. Neirotti, F. Calvo, D. L. Freeman, and J. D. Doll, J. Chem. Phys. **112**, 10 340 (2000).
[32] J. P. K. Doye and F. Calvo, Phys. Rev. Lett. **86**, 3570 (2001).
[33] F. Calvo, J. P. K. Doye, and D. J. Wales, Phys. Rev. Lett. **87**, 119301 (2001).
[34] W. Zhang, L. Liu, J. Zhuang, and Y. Li, Phys. Rev. B **62**, 8276 (2000).
[35] F. Baletto, C. Mottet, and R. Ferrando, Phys. Rev. B **63**, 155408 (2001).
[36] J. P. K. Doye, M. A. Miller, and D. J. Wales, J. Chem. Phys. **111**, 8417 (1999).
[37] J. A. Northby, J. Chem. Phys. **87**, 6166 (1987).
[38] D. J. Wales, J. Chem. Phys. **101**, 3750 (1994).
[39] M. A. Miller, J. P. K. Doye, and D. J. Wales, J. Chem. Phys. **110**, 328 (1999).
[40] M. A. Miller, J. P. K. Doye, and D. J. Wales, Phys. Rev. E **60**, 3701 (1999).
[41] L. J. Gallego, J. Garcia-Rodeja, M. M. G. Alemany, and C. Rey, Phys. Rev. Lett. **83**, 5258 (1999).
[42] J. M. Pacheco and J. P. Prates-Ramalho, Phys. Rev. Lett. **79**, 3873 (1997).
[43] F. Calvo, J. Phys. Chem. B **105**, 2183 (2001).
[44] Y.-H. Luo, J. Zhao, S. Qiu, and G. Wang, Phys. Rev. B **59**, 14 903 (1999).
[45] B. M. Axilrod and E. Teller, J. Chem. Phys. **11**, 299 (1943).
[46] D. J. Wales and J. Uppenbrink, Phys. Rev. B **50**, 12 342 (1994).
[47] M. H. J. Hagen and D. Frenkel, J. Chem. Phys. **101**, 4093 (1994).
[48] J. P. K. Doye and D. J. Wales, J. Chem. Soc., Faraday Trans. **93**, 4233 (1997).
[49] D. J. Wales, J. Chem. Soc., Faraday Trans. **86**, 3505 (1990).
[50] J. Uppenbrink and D. J. Wales, J. Chem. Phys. **96**, 8520 (1992).
[51] D. J. Wales and J. P. K. Doye, J. Phys. Chem. A **101**, 5111 (1997).
[52] Z. Li and H. A. Scheraga, Proc. Natl. Acad. Sci. U.S.A. **84**, 6611 (1987).
[53] D. J. Wales and H. A. Scheraga, Science **285**, 1368 (1999).
[54] J. P. K. Doye, D. J. Wales, and M. A. Miller, J. Chem. Phys. **109**, 8143 (1998).
[55] J. P. K. Doye, in *Global Optimization—Selected Case Studies*, edited by J. D. Pinter (Kluwer Academic, Dordrecht, in press); cond-mat/007338 (unpublished).
[56] B. Hartke, Chem. Phys. Lett. **258**, 144 (1996).
[57] J. P. K. Doye, Phys. Rev. E **62**, 8753 (2000).
[58] C. J. Cerjan and W. H. Miller, J. Chem. Phys. **75**, 2800 (1981).
[59] D. J. Wales *et al.*, Adv. Chem. Phys. **115**, 1 (2000).
[60] D. J. Wales, J. P. K. Doye, A. Dullweber, M. P. Hodges, F. Y. Naumkin, and F. Calvo, The Cambridge Cluster Database, URL http://www-wales.ch.cam.ac.uk/CCD.html
[61] F. Baletto, C. Mottet, and R. Ferrando, Phys. Rev. Lett. **84**, 5544 (2000).
[62] F. H. Stillinger and D. K. Stillinger, J. Chem. Phys. **93**, 6013 (1990).
[63] R. E. Kunz and R. S. Berry, Phys. Rev. Lett. **71**, 3987 (1993).
[64] O. M. Becker and M. Karplus, J. Chem. Phys. **106**, 1495 (1997).
[65] D. J. Wales, M. A. Miller, and T. R. Walsh, Nature (London) **394**, 758 (1998).
[66] P. E. Leopold, M. Montal, and J. N. Onuchic, Proc. Natl. Acad. Sci. U.S.A. **89**, 8271 (1992).
[67] J. D. Bryngelson, J. N. Onuchic, N. D. Socci, and P. G. Wolynes, Proteins: Struct., Funct., Genet. **21**, 167 (1995).
[68] D. R. Nelson and F. Spaepen, Solid State Phys. **42**, 1 (1989).
[69] D. J. Wales, Mol. Phys. **78**, 151 (1993).
[70] J. P. K. Doye and D. J. Wales, J. Chem. Phys. **102**, 9659 (1995).
[71] F. Calvo, J. P. K. Doye, and D. J. Wales, J. Chem. Phys. (to be published).
[72] E. Marinari and G. Parisi, Europhys. Lett. **19**, 451 (1992).

[73] R. H. Swendsen and J.-S. Wang, Phys. Rev. Lett. **57**, 2607 (1986).
[74] F. Calvo and J. P. K. Doye, Phys. Rev. E **63**, 010902(R) (2001).
[75] J. P. K. Doye and F. Calvo (unpublished).
[76] F. Baletto, J. P. K. Doye, and R. Ferrando (unpublished).
[77] A. Cheng and M. L. Klein, Phys. Rev. B **45**, 1889 (1992).
[78] M. S. Deleuze and F. Zerbetto, J. Am. Chem. Soc. **121**, 5281 (1999).
[79] Z. Gamba, Phys. Rev. B **57**, 1402 (1998).
[80] J. P. Lu, X.-P. Li, and R. M. Martin, Phys. Rev. Lett. **68**, 1551 (1992).
[81] M. Sprik, A. Cheng, and M. L. Klein, J. Phys. Chem. **96**, 2027 (1992).
[82] T. Yildirim, A. B. Harris, S. C. Erwin, and M. R. Pederson, Phys. Rev. B **48**, 1888 (1993).